

Many-body entanglement and spectral clusters in the extended hard-core bosonic Hatano-Nelson model

Chao-Ze Lu^{1, 2} and Gaoyong Sun^{1, 2, *}

¹College of Physics, Nanjing University of Aeronautics and Astronautics, Nanjing, 211106, China

²Key Laboratory of Aerospace Information Materials and Physics (NUAA), MIIT, Nanjing 211106, China

We study the many-body entanglement and spectra of the extended bosonic Hatano-Nelson model in the hard-core limit. We first show the quantum entanglement entropy can describe phase transitions for both the ground state and the first excited state. The phase transition of the ground state is second-order with the central charge $c = 1$. While the phase transition of the first excited state is the first-order \mathcal{PT} transition associated with a sudden change of the entanglement entropy. Secondly, we show that all energy spectral clusters would form ellipses in strong nearest-neighbor interactions, for which we establish a universal scaling law. The lengths of the major and minor axes are shown to obey power laws with respect to the nearest-neighbor interaction. Finally, we derive exact expressions for the numbers of energy levels on the outermost elliptic ring of each clusters.

I. INTRODUCTION

Quantum entanglement that is a central concept of quantum mechanics has broad potential applications, such as quantum teleportation [1], quantum computation [2, 3] and quantum sensing [4] in quantum technology and quantum information science [2, 5]. A notable application of the quantum entanglement for a many-body system is to characterize the equilibrium phase transition [6, 7], where the entanglement entropy was shown to display a logarithmic divergence in a one dimensional model [8]. Quantum entanglement is a crucial tool in understanding quantum phases of Hermitian many-body systems.

Non-Hermitian systems are of particular interest because of many unique phenomena that have no counterparts in Hermitian systems [9, 10]. It is known that non-Hermitian skin effects [11–25] and exceptional points [26–37] are two of fascinating phenomena in non-Hermitian systems. Recently, the entanglement entropy has been generalized to non-Hermitian systems for understanding phase transitions. For instance, the biorthogonal entanglement entropy is introduced to describe the equilibrium phase transitions [38–42], where the central charge is found to negative at an exceptional point from the entanglement entropy under specific treatments [38, 41, 42]. The negative central charge is argued to be described by the nonunitary conformal field theory [38, 41]. The understanding and the efficiently numerical computation of the entanglement entropy at an exceptional point is still an open question.

Many-body physics of non-Hermitian systems is another interesting topic, in which rich unique phenomena such as many-body skin effects [43–50], many-body edge bursts [51] and entanglement phase transitions [52–54] are explored in recent years. Concern for the many-body spectra [46, 47, 50] might be at the core of the researches

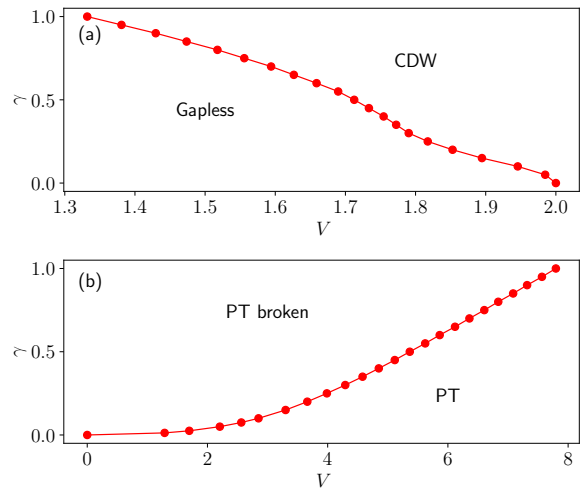


FIG. 1. Many-body phase diagram of the half-filled hard-core BHN model with respect to γ and V with $L = 20$ and $t = 1$ in PBCs, (a) The ground-state phase diagram, derived from the peak of the entanglement entropy, (b) The phase diagram of the first-excited state, obtained from the sudden change of the energy from a real value to a complex value.

as a direct extension of the single-particle physics. Recently, studies show that interaction can induce \mathcal{PT} transitions [47] and spectral structures [46, 47] in the interacting fermionic Hatano-Nelson (FHN) model in periodic boundary conditions (PBCs).

In order to further understand phase transitions and spectral structures induced by the interaction, we instead study the interacting bosonic Hatano-Nelson (BHN) model with a hard-core constraint, which cannot be equivalent to FHN under PBCs even in the thermodynamic limit [50]. We show that the BHN model undergoes a second-order phase transition in the ground state and a first-order parity-time (\mathcal{PT}) transition in the first excited state. The ground-state phase transition can be described by both the biorthogonal entanglement entropy and the self-norm entanglement entropy,

* Corresponding author: gysun@nuaa.edu.cn

from which the central charge $c = 1$ is derived. For the first-excited phase transition, we find that the self-norm entanglement entropy display a sudden change near the critical point, while the biorthogonal entanglement entropy become huge and meaningless in the case of small interactions. We argue that the meaningless values of the biorthogonal entanglement entropy come from the orthogonality of the biorthogonal eigenstates. We solve this problem by defining the biorthogonal entanglement entropy via the combination of eigenstates. In addition, we study the many-body energy spectra by increasing the interaction, where we find that the energy spectral clusters form ellipses in strong nearest-neighbor interactions. We establish the universal laws of spectral clusters, showing that the structure of an ellipse dependent on the interaction, the filling and the number of clusters.

This paper is organized as follows. In Sec. II, we introduce the bosonic Hatano-Nelson model. In Sec. III, we study the entanglement entropy of the ground state and the first excited state. In Sec. IV, we discuss the properties of spectral clusters in strong nearest-neighbor interactions. In Sec. V, we summarize our results.

II. MODEL

In this paper, we study the one-dimensional extended BHN model, which is a non-Hermitian system with a nearest-neighbor nonreciprocal hopping. The Hamiltonian of the extended BHN model can be written as,

$$\hat{H} = \sum_{l=1}^L [(t+\gamma)\hat{b}_l^\dagger \hat{b}_{l+1} + (t-\gamma)\hat{b}_{l+1}^\dagger \hat{b}_l + \frac{U}{2}\hat{n}_l(\hat{n}_l-1) + V\hat{n}_l\hat{n}_{l+1}], \quad (1)$$

where $\hat{b}_l^\dagger(\hat{b}_l)$ is the creation (annihilation) operator of a boson at the lattice site l , and $\hat{n}_l = \hat{b}_l^\dagger \hat{b}_l$ is the bosonic number operator. L is the length of the chain. The real parameters t and γ denote the reciprocal and nonreciprocal hopping coefficients of bosons between two nearest neighboring sites, respectively. The coupling coefficient U is the on-site interaction, and V is the nearest-neighbor interaction between two bosons in adjacent lattice sites. The PBCs is imposed by $b_{L+1} = b_1$.

Because it is extremely difficult to diagonalize a huge non-Hermitian matrix, numerical simulations of soft-core bosons is beyond the scope of the exact diagonalization method. In the following, we will study the system with the exact diagonalization in PBCs and merely consider the system with a hard-core constraint ($U \rightarrow \infty$). The extended BHN model in the hard-core limit is given by,

$$\hat{H} = \sum_l [(t+\gamma)\hat{b}_l^\dagger \hat{b}_{l+1} + (t-\gamma)\hat{b}_{l+1}^\dagger \hat{b}_l + V\hat{n}_l\hat{n}_{l+1}], \quad (2)$$

with a constraint $\hat{n}_l = \{0, 1\}$. The BHN model in the hard-core limit is equivalent to the FHN model in OBCs [47], but is different from the FHN model in PBCs [50]. Consequently, the eigenvalues of Eq.(2) are always real

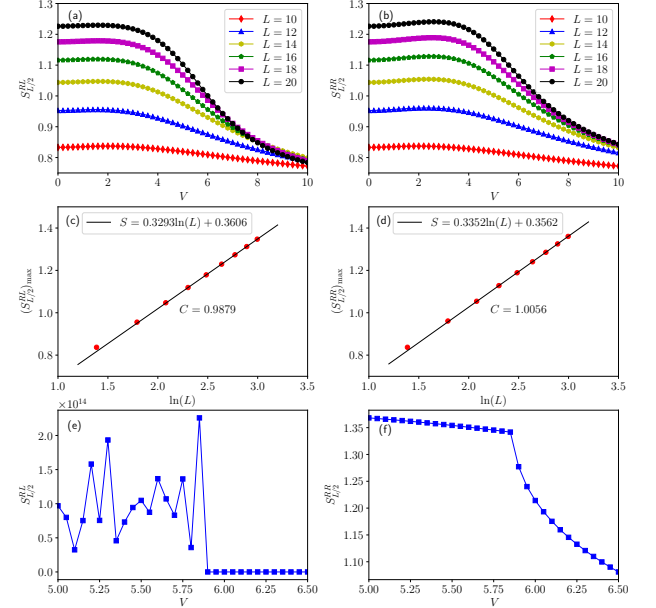


FIG. 2. Half-chain entanglement entropy of the half-filled BHN model at $t = 1$ and $\gamma = 0.6$ in PBCs. (a)(b) The biorthogonal and the self-norm entanglement entropy of the ground state as the function of V , (c)(d) The scaling of the maxima of biorthogonal and the self-norm entanglement entropy of the ground state, (e)(f) The biorthogonal and the self-norm entanglement entropy of the first-excited state.

for $\gamma < t$ in OBCs as the Hamiltonian can be mapped to a Hermitian Hamiltonian under a site-dependent similarity transform [50]. In the following, we will set $t = 1$ during the simulations and consider the system expressed in Eq.(2) with PBCs as we are only interested in properties of the complex-valued energy spectra.

III. ENTANGLEMENT ENTROPY

A. Ground-state phase transitions

In half filling, the extended hard-core BHN can be mapped to the spin-1/2 chain,

$$\hat{H} = \sum_l [\frac{t}{2}(\sigma_l^x \sigma_{l+1}^x + \sigma_l^y \sigma_{l+1}^y) + \frac{V}{4}\sigma_l^z \sigma_{l+1}^z + i\frac{\gamma}{2}(\sigma_l^x \sigma_{l+1}^y - \sigma_l^y \sigma_{l+1}^x) - \frac{V}{2}\sigma_l^z + \frac{V}{4}], \quad (3)$$

by performing the transformations between the bosonic operators and the spin operators,

$$\sigma_l^+ = b_l, \quad (4)$$

$$\sigma_l^- = b_l^\dagger, \quad (5)$$

$$\sigma_l^z = 1 - 2b_l^\dagger b_l, \quad (6)$$

where $\sigma_l^+ = (\sigma_l^x + \sigma_l^y)/2$, $\sigma_l^- = (\sigma_l^x - \sigma_l^y)/2$ are raising and lowering operators, and $\sigma_l^x, \sigma_l^y, \sigma_l^z$ are Pauli matrices.

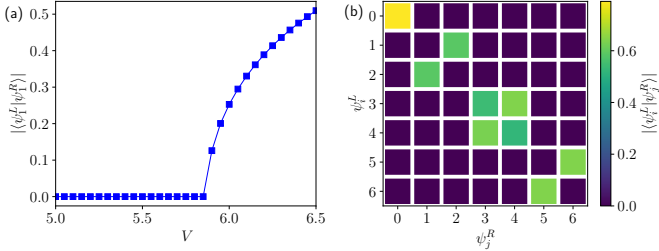


FIG. 3. The overlap of the left and right eigenstates of the half-filled BHN model with $L = 20$ at $t = 1$ and $\gamma = 0.6$ in PBCs. (a) The overlap of the left and right eigenstates of the first-excited state. (b) The overlap of the left and right eigenstates of the seven lowest states at $V = 5$.

In the case of $\gamma = 0$, the model in Eq.(3) is the well-known (Hermitian) XXZ model, which undergoes the Berezinskii-Kosterlitz-Thouless (BKT) transition between the doubly degenerated antiferromagnetic phase and the gapless XY phase. In boson language, such two ground states are named as the charge density wave (CDW) phase and the gapless phase (c.f. Fig.1(a)). In order to describe the phase transition, we introduce the entanglement entropy between part A and part B ,

$$S_A = -\text{Tr}_A(\rho_A \ln \rho_A), \quad (7)$$

where $\rho_A = \text{Tr}_B(|\psi_0\rangle\langle\psi_0|)$, and $|\psi_0\rangle$ is the ground state of the XXZ model. In the following, we choose the subsystems $A = \{1, \dots, L/2\}$ and $B = \{L/2 + 1, \dots, L\}$. For a Hermitian system, it is shown that the entanglement entropy scales logarithmically as [55],

$$S_{L/2} \propto \frac{c}{3} \ln(L) \quad (8)$$

at the critical point of a finite-size chain. The central charge $c = 1$ for the XXZ model that can be described by the conformal field theory (CFT) [55].

When $\gamma \neq 0$, the model in Eq.(3) is the generalized XXZ model with a complex Dzyaloshinskii-Moriya interaction (DMI), which is a non-Hermitian system. To verify whether the entanglement can describe the phase transition of the ground state (the state with a lowest real part) for such a non-Hermitian XXZ chain, we compute both the biorthogonal entanglement entropy $S_{L/2}^{RL}$ and the self-norm entanglement entropy $S_{L/2}^{RR}$. The biorthogonal and self-norm reduced density matrix are defined by the combination of the biorthogonal eigenstates $\rho_A^{RL} = \text{Tr}_B(|\psi_0^R\rangle\langle\psi_0^L|)$ and only the right density matrix $\rho_A^{RR} = \text{Tr}_B(|\psi_0^R\rangle\langle\psi_0^R|)$, respectively. Interestingly, we find that both $S_{L/2}^{RL}$ and $S_{L/2}^{RR}$ can describe the ground-state phase transition, which is a continuous phase transition with a central charge $c = 1$ as the Hermitian XXZ model ((c.f. Fig.2(a)(b)(c)(d))). The global ground-state phase diagram of the non-Hermitian XXZ is demonstrated in Fig.1(a), where we find that the complex DMI can introduce a gapped CDW phase even for a

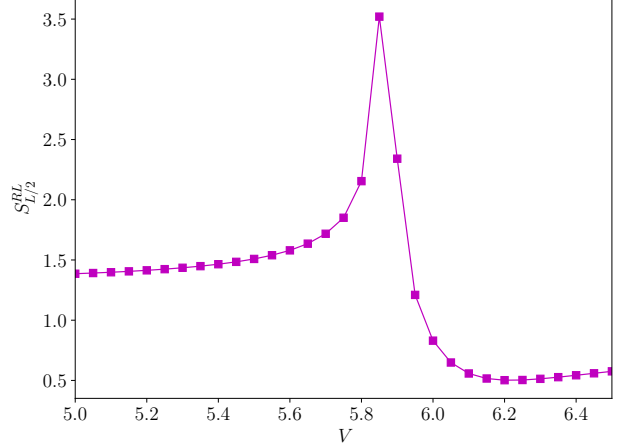


FIG. 4. The modified entanglement entropy of the first-excited state in the half-filled BHN model with $L = 20$ at $t = 1$ and $\gamma = 0.6$ in PBC. The density matrix are $\rho_1 = |\psi_1^R\rangle\langle\psi_2^L|$ and $\rho_1 = |\psi_1^R\rangle\langle\psi_1^L|$ in the regimes of the left side and right side of the peak, respectively.

weak interaction V compared to the original Hermitian XXZ model. This indicates that one could prepare a low-entangled ordered phase through the nonhermiticity.

B. \mathcal{PT} phase transitions

The BHN model in Eq.(2) (or in Eq.(3)) has a \mathcal{PT} symmetry, the system thus exists either real eigenenergies or complex eigenenergies in conjugated pairs. Consequently, in addition to the ground-state phase transition, the BHN model can in principle exhibit a \mathcal{PT} transition. A first-order \mathcal{PT} transition in the first-excited state has recently been discussed in the Ref.[47] for the FHN model. The global phase diagram of the first-excited state in the BHN model we considered is presented in Fig.1(b). In this section, we will instead investigate the properties of the quantum entanglement for such a \mathcal{PT} transition.

To achieve it, we calculate both the biorthogonal entanglement entropy $S_{L/2}^{RL}$ and self-norm entanglement entropy $S_{L/2}^{RR}$ for the first-excited state. We surprisingly find that $S_{L/2}^{RR}$ exhibits a sudden change when changing the interaction, however $S_{L/2}^{RL}$ has a huge and meaningless value in the small interaction as demonstrated in Fig.2(e)(f). It is argued that the meaningless value of $S_{L/2}^{RL}$ comes from the orthogonality of the biorthogonal eigenstates as shown in Fig.3(a). The orthogonality of the left and right eigenstates of the same real energy is found common for this model (c.f. Fig.3(b)). Moreover, we find that the left and right eigenstates of the different real energies can be nonorthogonal (c.f. Fig.3(b)), indicating that one may solve this problem by redefining the biorthogonal entanglement entropy by using the combination of eigenstates. We present the results of the modified $S_{L/2}^{RL}$ in Fig.4, where $S_{L/2}^{RL}$ exhibits a smooth

curve with a perfect peak located at the critical point.

We have to point out that it is impossible to extract the critical exponents using the modified $S_{L/2}^{RL}$ in Fig.4 or $S_{L/2}^{RR}$ in Fig.2(e). The study of exceptional points from the finite-size scaling of entanglement entropy is open. Unfortunately, our finding indicates that the problem could be more difficult to handle as the left and right eigenstates can be unexpectedly orthogonal.

IV. SPECTRAL CLUSTERS

It is easy to show that the energy spectrum which can be exactly obtained for the BHN model is a simple closed curve in the case of noninteractions [47, 50]. However, the spectrum structure is too complicated to know for the BHN model under interactions. Recently, it was found interestingly that the energy spectrum of the FHN model away from half filling would be separated into spectral clusters [c.f. Fig.5(a)(b)(c)] when the interaction strength V is larger than the range of each cluster [47]. It is worth while to note that energy spectra can also form clusters even in half filling, which is not discussed in Ref.[47]. The spectral clusters in half filling would be located only in the real-energy axis as energies are always real under strong interactions. In this following, we will study the properties of energy spectral structures in the BHN model with strong interactions to investigate whether more universal structures of energy spectra exist.

It can be seen from the Fig.5(a)(b)(c) that the energy spectrum is symmetrically distributed in the complex plane [47]. Assume the system has N particle numbers, the energy spectrum would form N clusters. The central position of each cluster E_c is round $(n_s - 1)V$. Here, we use n_s , with $n_s = 1, \dots, N$, to label these clusters individually. As the system has a particle-hole symmetry, the properties of clusters for $L - N$ particles are the same as those for N particles. Let us first study the central positions E_c of these energy clusters. We note that the central positions of these clusters are not exactly located at $(n_s - 1)V$. Instead, they are [47],

$$E_c = (n_s - 1)V + \varepsilon, \quad (9)$$

with,

$$\varepsilon \approx C(t^2 - \gamma^2). \quad (10)$$

It was shown that $C = 2/V$ in Ref.[47]. However, we argue that this coefficient is not universal for half filling. For example, in half filling, $C = 2/V$ for the cluster $n_s = N$, but $C = -L/V$ for the cluster $n_s = 1$. Moreover, we find that C is a quadratic function with respect to n_s for other cases. The coefficient C and the relation $n_s - N$ is found to satisfy the quadratic function,

$$C = -0.02(n_s - N)^2 - 0.03(n_s - N) + 0.05, \quad (11)$$

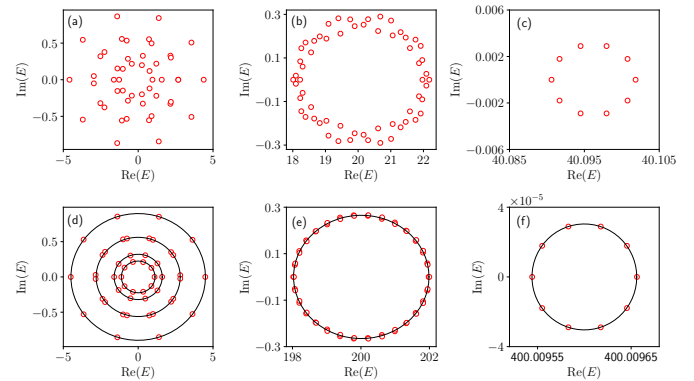


FIG. 5. The spectral clusters of the BHN model with $L = 10$ and $N = 3$ at $t = 1$ and $\gamma = 0.2$. (a)(b)(c) Spectral clusters for $n_s = 1, 2, 3$ and $V = 20$, (d)(e)(f) spectral clusters for $n_s = 1, 2, 3$ and $V = 200$.

approximatively. The argument is verified by numerical simulation using $L = 12$ at $V = 40$ in half filling, where we numerically find that $C = 0.05009 \approx 2/V$ when $n_s = N$, and $C = -0.2994 \approx -L/V$ when $n_s = 1$.

Next, we turn to study the shapes of clusters. Interestingly, we find that all spectral clusters would form perfect ellipses if the interaction V is strongly enough [c.f. Fig.5(d)(e)(f)]. Let us first discuss the rightmost cluster ($n_s = N$) that is a simple case as shown in Fig.5(f). We fit the data shown in Fig.5(f), finding that the function is an elliptic curve,

$$\frac{(x - x_0)^2}{a^2} + \frac{y^2}{b^2} = 1, \quad (12)$$

with the fitting parameters are $x_0 \approx 400.0096$, $a \approx 5.6001 \times 10^{-5}$, and $b \approx 3.0401 \times 10^{-5}$. Here, $2a$ and $2b$ are the lengths of the major and minor axes of the ellipse, $x_0 = E_c$ is the position of the centre of the ellipse, which satisfies $x_0 = (n_s - 1)V + 2(t^2 - \gamma^2)/V$.

We are surprised to find that the major axis $2a$ and minor axis $2b$ obey a universal scaling [c.f. Fig.6], which satisfies the following relation,

$$2a = C_a V^{p_a} + V_{0a}, \quad (13)$$

$$2b = C_b V^{p_b} + V_{0b}, \quad (14)$$

where C_a , C_b , p_a , p_b , V_{0a} and V_{0b} are fitting parameters. To obtain the accurate values of C_a , C_b , p_a and p_b , we fit the major and minor axes $2a$ and $2b$ with respect to V of the rightmost cluster for $L = 10, 12, 14$ and $n_s = N$. The fitting results are shown in Table A1 [see Appendix A for details], where we find that when the system is away from the half filling, the parameters C_a , C_b , p_a and p_b are given as,

$$C_a = 2[(t + \gamma)^N + (t - \gamma)^N], \quad p_a = 1 - N, \quad (15)$$

$$C_b = 2[(t + \gamma)^N - (t - \gamma)^N], \quad p_b = 1 - N. \quad (16)$$

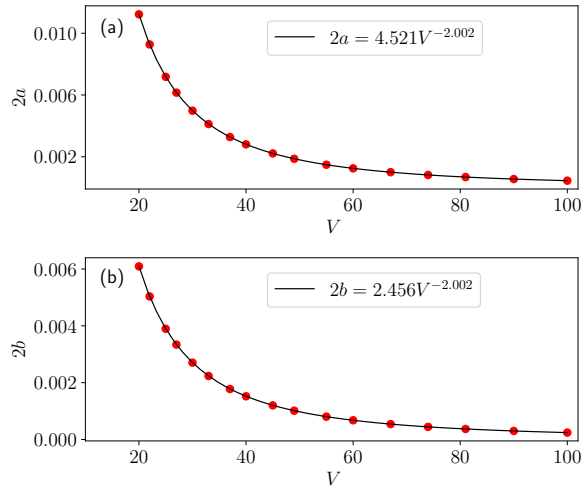


FIG. 6. The major and minor axes of the ellipse of the third cluster ($n_s = 3$) in the BHN model with $L = 10$ and $N = 3$ particles at $t = 1$ and $\gamma = 0.2$.

Above scaling exponents can be obtained from the perturbation theory [47]. While when the system is prepared in the half filling, the eigenenergies are always real for large interactions, thus there are only two fitting parameters for the major axis, which are given by,

$$C_a = 4[(t + \gamma)^N + (t - \gamma)^N], \quad p_a = 1 - N. \quad (17)$$

Here, $V_{0a} = V_{0b} = 0$ for an arbitrary filling.

To verify whether the scaling exponents p_a, p_b obtained for $n_s = N$ are valid for other clusters, we study the properties of the first cluster ($n_s = 1$). It can be seen from Fig. 5(d), the energy spectrum forms parallel ellipses for the first cluster. The major axis $2a$ and minor axis $2b$ of the outermost ellipse are numerically fitted by using the Eq.(13) and Eq.(14). The parameters $C_a, C_b, p_a, p_b, V_{0a}$ and V_{0b} are shown in Table A2 [see Appendix A for details], where we find that p_a and p_b remain,

$$p_a = p_b = 1 - N, \quad (18)$$

for the half-filled system, while if the system is away from the half filling except the single particle ($N = 1$) case, p_a and p_b are,

$$p_a = p_b = -2. \quad (19)$$

Moreover, for more general cases, that is $2 \leq n_s \leq N - 1$, we find that the scaling exponents p_a and p_b may satisfy,

$$p_a = p_b = 1 - n_s. \quad (20)$$

for all fillings. However, we have to note that there are several exceptions where p_a and p_b are not consistent with this scaling rule in Eq.(20), which we think may be due to the instability of the numerical simulations. This problem is left for future study.

Finally, we investigate the numbers of energy levels on a single elliptic ring. It is found that energy levels distribute symmetrically in the elliptic lines, in which the number of the levels N_q is related to the chain length L . We find that the number of levels N_q on the outermost elliptic ring of each clusters is,

$$N_q = L, \quad (21)$$

for the clusters $n_s = 1$ and $n_s = N$. While for other clusters $2 \leq n_s \leq N - 1$, the number of energy levels N_q is given by,

$$N_q = (n_s + L/2 - N - 1)L, \quad (22)$$

dependent on L, N and n_s . The energy values E on the outermost ellipse can be derived as,

$$E(q) = E_c + a \cos(q) + ib \sin(q), \quad (23)$$

with $q = 2n\pi/N_q$, and $n = 0, 1, \dots, N_q - 1$. The energy spectrum in Eq.(23) is similar to the single-particle energy spectrum, indicating that one may analyze the many-body physics using the concepts or techniques from the single-particle picture. In addition, universal properties of many-body systems under intermediate interactions is completely unknown so far, which is beyond the scope of this work and left for future research.

V. CONCLUSION

We have studied the entanglement entropy and spectral clusters of the extended hard-core BHN model in PBCs. We show that the extended hard-core BHN model undergoes a second-order phase transition in the ground state that can be described by both the biorthogonal and self-norm entanglement entropy in addition to the first-order \mathcal{PT} transition of the first-excited state discussed in FHN model [47]. However, for the first-order \mathcal{PT} transition, we find that the biorthogonal entanglement entropy cannot characterize the transition because of the orthogonality of the left and right eigenstates. We solve this problem by redefining the entanglement entropy.

Moreover, we investigate the properties of the energy eigenvalues of each clusters led by the interaction, finding that the shape of each cluster is an elliptic function when the nearest-neighbor interaction is strongly enough. We summarized the relationship between the size of the ellipses of each cluster and corresponding parameters, deriving the universal scaling laws for each of ellipses. Finally, we analyze the number of energy levels of each ellipse, finding a universal express of the number of levels for the outermost circles of clusters.

ACKNOWLEDGMENTS

This work is supported by "the Fundamental Research Funds for the Central Universities, NO. NS2023055" and

is partially supported by the High Performance Comput-

ing Platform of Nanjing University of Aeronautics and Astronautics.

[1] D. Bouwmeester, J.-W. Pan, K. Mattle, M. Eibl, H. Weinfurter, and A. Zeilinger, *Nature* **390**, 575 (1997).

[2] M. A. Nielsen and I. L. Chuang, *Quantum computation and quantum information* (Cambridge University Press, 2010).

[3] R. Jozsa and N. Linden, *Proceedings of the Royal Society of London. Series A: Mathematical, Physical and Engineering Sciences* **459**, 2011 (2003).

[4] C. L. Degen, F. Reinhard, and P. Cappellaro, *Reviews of Modern Physics* **89**, 035002 (2017).

[5] R. Horodecki, P. Horodecki, M. Horodecki, and K. Horodecki, *Reviews of Modern Physics* **81**, 865 (2009).

[6] A. Osterloh, L. Amico, G. Falci, and R. Fazio, *Nature* **416**, 608 (2002).

[7] J. Eisert, M. Cramer, and M. B. Plenio, *Reviews of Modern Physics* **82**, 277 (2010).

[8] G. Vidal, J. I. Latorre, E. Rico, and A. Kitaev, *Physical Review Letters* **90**, 227902 (2003).

[9] E. J. Bergholtz, J. C. Budich, and F. K. Kunst, *Reviews of Modern Physics* **93**, 015005 (2021).

[10] Y. Ashida, Z. Gong, and M. Ueda, *Advances in Physics* **69**, 249 (2021).

[11] T. E. Lee, *Physical Review Letters* **116**, 133903 (2016).

[12] S. Yao and Z. Wang, *Physical Review Letters* **121**, 086803 (2018).

[13] F. K. Kunst, E. Edvardsson, J. C. Budich, and E. J. Bergholtz, *Physical Review Letters* **121**, 026808 (2018).

[14] Y. Xiong, *Journal of Physics Communications* **2**, 035043 (2018).

[15] Z. Gong, Y. Ashida, K. Kawabata, K. Takasan, S. Higashikawa, and M. Ueda, *Physical Review X* **8**, 031079 (2018).

[16] V. M. Martinez Alvarez, J. E. Barrios Vargas, and L. E. F. Foa Torres, *Physical Review B* **97**, 121401(R) (2018).

[17] K. Yokomizo and S. Murakami, *Physical Review Letters* **123**, 066404 (2019).

[18] N. Okuma, K. Kawabata, K. Shiozaki, and M. Sato, *Physical Review Letters* **124**, 086801 (2020).

[19] K. Zhang, Z. Yang, and C. Fang, *Physical Review Letters* **125**, 126402 (2020).

[20] Z. Yang, K. Zhang, C. Fang, and J. Hu, *Physical Review Letters* **125**, 226402 (2020).

[21] X.-R. Wang, C.-X. Guo, and S.-P. Kou, *Physical Review B* **101**, 121116(R) (2020).

[22] H. Jiang, R. Lü, and S. Chen, *The European Physical Journal B* **93**, 1 (2020).

[23] S. Weidemann, M. Kremer, T. Helbig, T. Hofmann, A. Stegmaier, M. Greiter, R. Thomale, and A. Szameit, *Science* **368**, 311 (2020).

[24] L. Xiao, T. Deng, K. Wang, G. Zhu, Z. Wang, W. Yi, and P. Xue, *Nature Physics* **16**, 761 (2020).

[25] D. S. Borgnia, A. J. Kruchkov, and R.-J. Slager, *Physical Review Letters* **124**, 056802 (2020).

[26] W. Heiss, *Journal of Physics A: Mathematical and Theoretical* **45**, 444016 (2012).

[27] V. Kozii and L. Fu, *arXiv preprint arXiv:1708.05841* (2017).

[28] H. Hodaei, A. U. Hassan, S. Wittek, H. Garcia-Gracia, R. El-Ganainy, D. N. Christodoulides, and M. Khajavikhan, *Nature* **548**, 187 (2017).

[29] H. Zhou, C. Peng, Y. Yoon, C. W. Hsu, K. A. Nelson, L. Fu, J. D. Joannopoulos, M. Soljačić, and B. Zhen, *Science* **359**, 1009 (2018).

[30] M.-A. Miri and A. Alu, *Science* **363**, 42 (2019).

[31] J.-H. Park, A. Ndao, W. Cai, L.-Y. Hsu, A. Kodigala, T. Lepetit, Y.-H. Lo, and B. Kanté, *arXiv preprint arXiv:1904.01073* (2019).

[32] Z. Yang and J. Hu, *Physical Review B* **99**, 081102(R) (2019).

[33] Ş. Özdemir, S. Rotter, F. Nori, and L. Yang, *Nature Materials* **18**, 783 (2019).

[34] B. Dóra, M. Heyl, and R. Moessner, *Nature Communications* **10**, 1 (2019).

[35] L. Jin, H. C. Wu, B.-B. Wei, and Z. Song, *Physical Review B* **101**, 045130 (2020).

[36] L. Xiao, T. Deng, K. Wang, Z. Wang, W. Yi, and P. Xue, *Physical Review Letters* **126**, 230402 (2021).

[37] C. Chen, Y. Liu, L. Zhao, X. Hu, and Y. Fu, *Frontiers of Physics* **17**, 52504 (2022).

[38] P.-Y. Chang, J.-S. You, X. Wen, and S. Ryu, *Physical Review Research* **2**, 033069 (2020).

[39] Y.-B. Guo, Y.-C. Yu, R.-Z. Huang, L.-P. Yang, R.-Z. Chi, H.-J. Liao, and T. Xiang, *Journal of Physics: Condensed Matter* **33**, 475502 (2021).

[40] L.-M. Chen, Y. Zhou, S. A. Chen, and P. Ye, *Physical Review B* **105**, L121115 (2022).

[41] T. Sanno, M. G. Yamada, T. Mizushima, and S. Fujimoto, *Physical Review B* **106**, 174517 (2022).

[42] Y.-T. Tu, Y.-C. Tzeng, and P.-Y. Chang, *SciPost Physics* **12**, 194 (2022).

[43] D.-W. Zhang, Y.-L. Chen, G.-Q. Zhang, L.-J. Lang, Z. Li, and S.-L. Zhu, *Physical Review B* **101**, 235150 (2020).

[44] S. Mu, C. H. Lee, L. Li, and J. Gong, *Physical Review B* **102**, 081115(R) (2020).

[45] C. H. Lee, *Physical Review B* **104**, 195102 (2021).

[46] K. Kawabata, K. Shiozaki, and S. Ryu, *Physical Review B* **105**, 165137 (2022).

[47] S.-B. Zhang, M. M. Denner, T. Bzdušek, M. A. Sentef, and T. Neupert, *Physical Review B* **106**, L121102 (2022).

[48] F. Alsallom, L. Herviou, O. V. Yazyev, and M. Brzezínska, *Physical Review Research* **4**, 033122 (2022).

[49] R. Shen and C. H. Lee, *Communications Physics* **5**, 238 (2022).

[50] G. Sun and S.-P. Kou, *arXiv:2307.04696* (2023).

[51] Y.-M. Hu, W.-T. Xue, F. Song, and Z. Wang, *arXiv:2306.08676* (2023).

[52] K. Kawabata, T. Numasawa, and S. Ryu, *Physical Review X* **13**, 021007 (2023).

[53] X. Feng, S. Liu, S. Chen, and W. Guo, *Physical Review B* **107**, 094309 (2023).

[54] S.-Z. Li, X.-J. Yu, and Z. Li, *arXiv:2309.03546* (2023).

[55] P. Calabrese and J. Cardy, *Journal of Statistical Mechanics: Theory and Experiment* **2004**, P06002 (2004).

Appendix A: Numerical data for $n_s = N$ and $n_s = 1$

In the appendix, we display the data for $n_s = N$ in Table A1 and $n_s = 1$ in Table A2, respectively.

TABLE A1. The fitting parameters of the major and minor axes $2a$ and $2b$ with respect to V for the cluster $n_s = N$ with $L = 10, 12, 14$, $t = 1$ and $\gamma = 0.2$.

L	N	$1 - n_s$	C_a	p_a	C_b	p_b
10	1	-0	4.000	-0.000	0.800	-0.000
10	2	-1	4.160	-1.000	1.600	-1.000
10	3	-2	4.511	-2.002	2.449	-2.002
10	4	-3	5.085	-3.005	3.335	-3.000
10	5	-4	11.51	-4.005	-	-
12	1	-0	4.000	-0.000	0.800	-0.000
12	2	-1	4.160	-1.000	1.600	-1.000
12	3	-2	4.511	-2.002	2.449	-2.002
12	4	-3	5.037	-3.003	3.338	-3.003
12	5	-4	5.810	-4.007	4.363	-4.002
12	6	-5	13.13	-5.000	-	-
14	1	-0	4.000	-0.000	0.807	-0.000
14	2	-1	4.160	-1.000	1.615	-1.000
14	3	-2	4.511	-2.002	2.449	-2.002
14	4	-3	5.037	-3.003	3.338	-3.003
14	5	-4	5.753	-4.005	4.410	-4.005
14	6	-5	6.582	-5.000	5.657	-5.011
14	7	-6	20.23	-6.102	-	-

TABLE A2. The fitting parameters of the major and minor axes $2a$ and $2b$ with respect to V for the cluster $n_s = 1$ with $L = 6, 8, 10, 12, 14$, $t = 1$ and $\gamma = 0.2$.

L	N	$1 - N$	C_a	p_a	V_{0a}	C_b	p_b	V_{0b}
6	1	-0	0.000	-0.000	4.000	0.000	0.000	0.800
6	2	-1	-9.353	-1.981	5.657	0.079	-2.000	1.131
6	3	-2	24.02	-1.971	0.000	-	-	-
8	1	-0	0.000	-0.000	4.000	0.000	0.000	0.800
8	2	-1	-3.347	-1.987	6.928	0.0277	-2.000	1.386
8	3	-2	-10.40	-1.971	6.472	-2.930	-1.995	1.294
8	4	-3	85.24	-2.961	0.000	-	-	-
10	1	-0	0.000	0.000	4.000	0.000	0.000	0.800
10	2	-1	-1.414	-1.981	7.391	0.012	-1.999	1.478
10	3	-2	-8.823	-1.995	8.988	-0.5964	-2.005	1.798
10	4	-3	-11.36	-1.994	6.928	-5.357	-1.992	1.386
10	5	-4	327.1	-3.952	0.000	-	-	-
12	1	-0	-0.000	-0.000	4.000	0.000	-0.000	0.800
12	2	-1	-0.7716	-2.004	7.608	0.0056	-1.977	1.522
12	3	-2	-5.207	-1.999	10.13	-0.1478	-2.000	2.026
12	4	-3	-13.72	-1.994	10.45	-1.947	-1.997	2.091
12	5	-4	-11.06	-2.000	7.208	-7.164	-1.995	1.442
12	6	-5	1830	-5.112	0.000	-	-	-
14	1	-0	-0.000	-0.000	4.000	-0.000	-0.000	0.800
14	2	-1	-0.446	-2.007	7.727	0.0034	-1.994	1.545
14	3	-2	-3.083	-1.999	10.73	-0.0416	-1.986	2.146
14	4	-3	-10.27	-2.001	12.31	0.5316	-1.914	2.462
14	5	-4	-17.25	-1.992	11.52	-3.846	-2.002	2.304
14	6	-5	-10.42	-2.001	7.391	-8.628	-2.000	1.478
14	7	-6	15693	-6.245	0.000	-	-	-